International Journal of Heat and Technology
Vol. 43, No. 5, October, 2025, pp. 1644-1656
Journal homepage: http://iieta.org/journals/ijht

Comparing Thermocapillary Bubble Migration in Normal and Zero Gravity in Small-Scale Containers

Yousuf Alhendal*, Mohammad Alhamli

Mechanical Power and Refrigeration Department (MPR), College of Technological Studies (CTS), Public Authority for Applied Education and Training (PAAET), Kuwait 70030, Kuwait

Corresponding Author Email: ya.alhendal@paaet.edu.kw

https://doi.org/10.18280/ijht.430503

Received: 20 August 2025
Revised: 12 October 2025
Accepted: 19 October 2025
Available online: 31 October 2025

Keywords:
bubble migration, gravitational force, convective capillary, Marangoni flow, thermocapillary, two-phase, VOF method

ABSTRACT

Thermocapillary migration under gravity and zero-gravity conditions was simulated using the Volume of Fluid (VOF) method in ANSYS Fluent software. The migration of a nitrogen bubble in a container filled with liquid ethanol was investigated numerically. Three distinct conditions were used to study the bubble migration in a compact container: gravity, thermocapillary, or both. According to the findings, buoyancy controls bubble migration in larger containers, while thermocapillary forces govern motion only at small scales (below 10 mm), showing an inverse dependence on container dimension. In thermocapillary flow, the bubble maintained its spherical shape as it traveled. In the buoyancy force, the spherical bubble shape became oblate. The bubble in the combination of thermocapillary and buoyancy forces, in contrast to the other two scenarios, shifted from a spherical to an oblate shape as the container's size expanded. It subsequently ruptures before it reaches the heated surface. The significance of this study lies in its estimation of the Marangoni force's emergence, the gravitational force's effect disappearing, and the neglect of its calculations at extremely small measurements. It also helps build high-quality engineering equipment on a small scale.

1. INTRODUCTION

Understanding the dynamics of bubbles and droplets is crucial. It can assist in developing new equipment to either mitigate or control the effects of these bubbles in several industrial processes and even in space devices. Under the influence of gravity, bubbles can change shape and even break apart, complicating their movement and sometimes harming equipment [1, 2]. Therefore, controlling these bubbles can enhance various engineering applications, such as welding on Earth and heat/mass transfer operations in space [3, 4].

At first, bubble migration was investigated by Young et al. [5], who observed that the bubbles were moving to the warmer side when a temperature gradient was applied because of surface tension variation. This occurrence is known as thermocapillary / Marangoni. Hardy [6] also studied bubble motion under Marangoni and buoyancy forces. They presented the required temperature gradients to balance the two forces depending on the bubble diameter. Bratukhin et al. [7] investigated Marangoni migration in normal gravity, with different techniques. Time, heat, and mass diffusion, as well as surfactant absorption characterizing the Marangoni convection, were analyzed. In fact, with the presence of gravity on Earth, natural convection occurs rapidly, which overpowers the Marangoni force [8]. Generally, in order to notice the Marangoni effect clearly, micro or zero gravity environments are used [9-13]. Wozniak et al. [14] described the temperature field surrounding a moving bubble in a reduced gravity environment. Some discrepancies were observed between numerical and experimental results due to some assumptions considered in the numerical study, as well as optical disturbances in the experiment.

Most of the studies were experimental. However, measurements are sometimes difficult to realize and very expensive, which pushed researchers to model and simulate the phenomenon as well as compare both numerical and experimental data to each other. Brackbill et al. [15] suggested a method to model surface tension based on the interface curvature, which simplifies the calculations. Thus, many researchers adopted it to construct their numerical model [16-18]. Moreover, the VOF method was found to be very reliable to describe two fluid flows, as shown in references [19-22]. Many numerical studies investigating one bubble migration as well as several bubbles were produced [23-25]. Mostly, when one bubble is migrating from cold to hot regions, it travels along a vertical path. However, it can have complex behavior, especially when it is subjected to other forces such as rotation [26-28] or vibration [29-32]. Those different trajectories have a direct impact on the arrival time of the bubble to the top; it is either delayed or advanced.

Another interesting parameter that affects bubble migration is the container's shape. Most of the articles were produced on cylindrical containers [33-35], unlike Balla et al. [36], who investigated a square channel container. Similar to the shape, the dimension of the container plays a crucial role. Both the distance that the bubble will travel and the sides of the

container will definitely impact the bubble's velocity and shape [37]. Therefore, this study examines and contrasts the motion and behavior of bubbles in small containers before progressively expanding their size in three scenarios: with the buoyancy force on its own, with the Marangoni effect, and with the Marangoni effect by itself. We concentrate on the level at which the buoyancy effect becomes apparent, which is noticeable and important, and the Marangoni effect starts to progressively disappear.

2. INITIAL CONDITIONS AND ASSUMPTIONS

Under gravity and in zero-gravity environment, the movement of a nitrogen bubble in an ethanol container is investigated (Figure 1). The container is heated from the top by T_{hot} = 325 K, while the bottom is maintained at T_{cold} = 300 K. The sidewalls are thermally isolated. The velocity is considered null on the walls. The bubble moves at a slow speed, and the flow remains laminar. Ethanol is an incompressible and Newtonian fluid; its thermophysical properties are considered to be unchanged except surface tension, σ, which depends on temperature. Prior to releasing the bubble, the steady-state temperature distribution is established at first in the container, and then it is considered as the initial condition for studying the unsteady motion of the bubble.

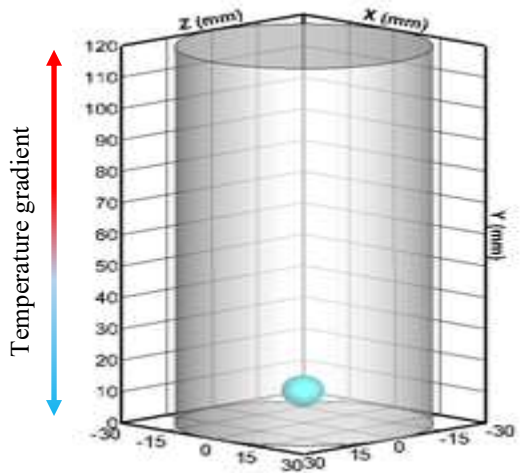

Figure 1. Geometry of the calculated field for thermocapillary migration

3. NUMERICAL MODEL

The YGB model is based on Young et al. [5] linear model:

$$V_{YGB} = \frac{2\left|\frac{d\sigma}{dT}\right| r_b \lambda \frac{dT}{dx}}{(2\mu + 3\mu')(2\lambda + \lambda')} \quad (1)$$

μ, μ', λ and λ' represent the dynamic viscosity and thermal conductivity, respectively, of the two phases (fluid and bubble).

Thermal Reynolds and Marangoni numbers are expressed as:

$$Re_T = \frac{r_b V_T}{\nu} \quad (2)$$

$$\mathrm{Ma_T} = \frac{\mathrm{r_b V_T}}{\alpha} = \mathrm{Re_T \cdot Pr} \quad (3)$$

V_T is the determined velocity from balancing tangential stresses at the free surface and is utilized to scale the velocity of migration (m/s) in Eqs. (2) and (3):

$$V_T = \frac{\frac{d\sigma}{dT}.\frac{dT}{dx}.r_b}{\mu} \quad (4)$$

with Prandtl number defined as:

$$\mathrm{Pr} = \frac{\nu}{\alpha} \quad (5)$$

α: thermal diffusivity and ν: kinematic viscosity:

$$\nu = \frac{\mu}{\rho} \quad (6)$$

with ρ, the density of the continuous phase fluid, and r_b is the bubble's radius, which is d/2, with d the bubble's diameter.

$d\sigma/dT$ or σ_T denotes the rate of change of interfacial tension, while dT/dx signifies the temperature gradient applied to the continuous phase fluid.

The governing continuum conservation equations for two-phase flow were solved using Ansys-Fluent software, and the volume of fluid (VOF) method was used to track the liquid/gas interface. The geometric reconstruction scheme, based on the piece-wise linear interface calculation (PLIC) method of Youngs [38] in Ansys-Fluent, was chosen for the current investigation. Geo-reconstruction is utilized to give more accuracy for free surface definition [19]. The movement of bubble-liquid interface is tracked depending on the gas bubble volume fraction distribution, i.e., α_G, in a computational cell, where the value of α_G is 0 for the liquid phase and 1 for the bubble phase. Therefore, a gas-liquid interface exists in the cell where α_G lies between 0 and 1.

The momentum equation, expressed below, is solved for all the phases existing in the domain:

$$\frac{\partial}{\partial t}(\rho\vec{v}) + \nabla.(\rho\vec{v}\vec{v}) = -\nabla p + \nabla.[\mu(\nabla\vec{v} + \nabla\vec{v}^T)] + \vec{F} + \rho\vec{g} \quad (7)$$

where, $\vec{v}$ is treated as the mass-averaged variable:

$$\vec{v} = \frac{\alpha_G\rho_G\vec{v}_G + \alpha_L\rho_L\vec{v}_L}{\rho} \quad (8)$$

When the zero environment is considered, $\vec{g}$ becomes null.

$\vec{F}$ represents surface tension force per unit volume. It is composed of normal force, $\overrightarrow{F_N}$, and tangential one, $\overrightarrow{F_T}$. Continuum surface force (CSF) model is used to compute it for the cells containing bubble-liquid interface [15]:

$$\overrightarrow{F_N} = \sigma\frac{\rho k\vec{n}}{\frac{1}{2}(\rho_L + \rho_G)} \quad (9)$$

where, σ is the coefficient of surface tension.

$$\sigma = \sigma_0 + \sigma_T(T_0 - T) \quad (10)$$

For the tangential surface tension force, it is defined as:

$$\overrightarrow{F_T} = -\sigma_T \nabla_s T \quad (11)$$

σ_0 represents the surface tension at a reference temperature T_0, T is the temperature of the liquid, $\vec{n}$ is the surface normal estimated from the volume fraction gradient, and k is the local surface curvature, defined as follows:

$$k = -(\nabla \hat{n}) = \frac{1}{|\vec{n}|}\left[\frac{\vec{n}}{|\vec{n}|}\nabla|\vec{n}| - (\nabla \square \vec{n})\right] \quad (12)$$

The interface tracking between bubble and liquid is achieved by the continuity equation solution for bubble volume fraction:

$$\frac{\partial}{\partial t}(\alpha_G \rho_G) + \nabla \cdot (\alpha_G \rho_G \vec{v}_G) = 0 \quad (13)$$

This equation is indirectly determined for the host fluid; instead, the volume fraction of the liquid is calculated as follows:

$$\alpha_G + \alpha_L = 1 \quad (14)$$

with α_G and α_L, volume fractions of the bubble and host-fluid, in that order. The density and viscosity of each cell at the interface are determined using the following expressions:

$$\rho = \alpha_G \rho_G + (1 - \alpha_G)\rho_L \quad (15)$$

$$\mu = \alpha_G \mu_G + (1 - \alpha_G)\mu_L \quad (16)$$

Under gravity force alone, $\vec{F}$ is assumed null. In that case, the velocity will be calculated from (7) in addition to continuity equation, expressed as:

$$\frac{\partial \rho}{\partial t} + \nabla(\rho \vec{v}) = 0 \quad (17)$$

For the only gravity case, the Peclet number is defined as:

$$\mathrm{Pe} = \frac{r_b V_g}{\nu \alpha} = Re.\ Pr \quad (18)$$

With V_g, the flow velocity takes into account only gravity. The equation of energy is also solved for all phases:

$$\frac{\partial}{\partial t}(\rho E) + \nabla.[\vec{v}(\rho E) + p)] = \nabla.(\kappa_{eff} \nabla T) \quad (19)$$

where, specific heat depends on the considered phase. Temperature, density ρ, and effective thermal conductivity k_{eff}, are shared by the phases.

VOF model treats energy (E) and temperature (T) as mass-averaged variables:

$$E = \frac{\sum_{q=1}^{n} \alpha_q \rho_q E_q}{\sum_{q=1}^{n} \alpha_q \rho_q} \quad (20)$$

GAMBIT was used to generate the finite-volume mesh before integrating it into Ansys-Fluent. The computations were conducted using a pressure-based, segregated, implicit solver. Pressure–velocity coupling was achieved using the pressure-implicit with splitting of operators (PISO), which applies two corrections for neighboring points and skewness. The pressure-staggering option (PRESTO) scheme was also used for pressure interpolation. Conservation equations were discretized using a second-order upwind differencing scheme. The time step used to obtain convergence is 10^{-2} s.

4. GRID SIZE DEPENDENCY

A nitrogen bubble was positioned at the center and 2xd from the bottom surface in liquid ethanol medium. In previous works [17, 21], thermocapillary model was already examined and validated properly with Thompson et al. [9]. As shown in Figure 2, the results are in good agreement with only minor discrepancies attributed to measurement and numerical errors. The accuracy of the simulation was attained by testing five grid meshes. Grid independence, mesh sizes, time steps, and extending the geometry to 3D were all checked to assure convergence. In this study, a grid consisting of 324,000 nodes, corresponding to 576 cells per bubble diameter, was considered for all simulations, owing to its accuracy in results while minimizing computing time and memory usage.

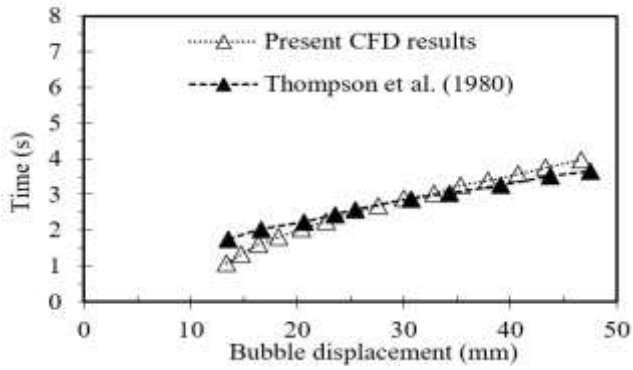

Figure 2. Present results validation with study [9]

5. THE PHENOMENON OF THERMOCAPILLARY BUBBLE DYNAMICS

For a container of 60mm diameter and 120mm height, when a temperature gradient is applied to a bubble N_2 (d = 8 mm) inside ethanol in zero gravity, this bubble moves in a vertical translation from the bottom (cold wall) to the top (hot wall). This result was already found by many researchers both experimentally and numerically [5, 9, 17, 29]. To investigate the behavior of thermocapillary bubble flow in zero gravity under a linear temperature distribution between the upper and lower walls, five different temperature differences were examined. Temperature changes of 2.5 K were made to the container's top, which ranged from 317.5 K to 325 K, while the container's bottom remained at 300 K. Obviously, for the higher T_{hot}, the bubble has already reached the top, while it is still in almost the middle of the container for the weakest T_{hot}. For all the cases, the isotherms behind the bubble are disturbed. Whenever the bubble is moving, a small recirculation of ethanol is created, which makes the temperature change in the medium. In fact, when T_{hot} increases, the bubble velocity

augments. Therefore, for a higher temperature gradient in the container, the bubble reaches the top rapidly, as indicated by the decreasing bubble arrival time (Figure 3). The Marangoni problem or thermocapillary migration problem are terms used to describe this kind of phenomenon.

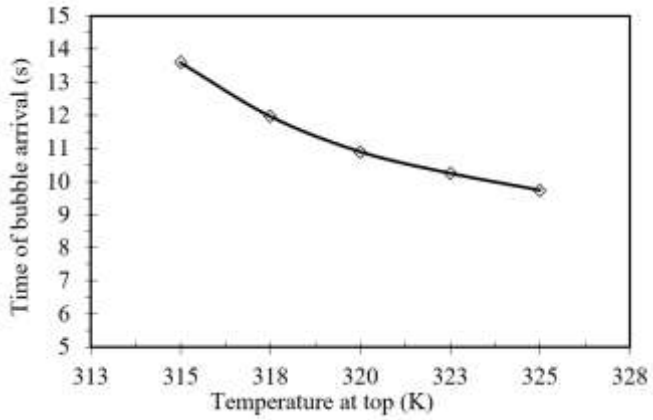

Figure 3. Bubble arrival time depending on T_{hot}

6. RESULTS AND DISCUSSION

This section investigates the impact of thermocapillary forces on bubble migration by varying container heights (h) and bubble radius (r_b) under three distinct conditions: normal gravity, normal gravity with thermocapillary effects, and zero gravity with thermocapillary effects. These conditions correspond to the following flow patterns: buoyancy-driven flow, combined buoyancy and thermocapillary flow, and thermocapillary-driven flow, as illustrated in Figure 4. Bubbles with a radius smaller than or equal to 0.24 mm exhibit no movement in cylinders less than 10mm in height under buoyancy-driven flow. Conversely, for the same cylinder height, in the presence of thermocapillary forces—whether gravity is applied or not—these bubbles consistently migrate toward the heated surface within the cylinder. The constant Ma_T, regardless of the presence or absence of gravity, suggests that the flow in these cases is dominated by thermocapillary effects alone. As r_b increases to 0.32 mm and h increases to 10mm, the bubble begins to migrate under all three flow conditions. However, under the combined buoyancy and thermocapillary flow, the migration pattern reveals noticeable deformation. As r_b and h increase further, this deformation becomes more pronounced in the presence of gravity and even more significant when both forces are acting together. In contrast, in the absence of gravity (thermocapillary flow), aside from slight elongation as the bubble migrates toward the heated surface, no deformation is observed. The interaction between gravity and thermocapillary forces significantly alters the bubble's shape. However, the effect of gravity alone on bubble deformation becomes more evident in larger bubbles. Due to their weight, these bubbles tend to flatten, as previously demonstrated by Cohen et al. [39] for large bubbles. For the three observed flow patterns, the bubble generally moves in a vertical trajectory. However, when h > 20 mm in buoyancy-driven flow, the bubble's trajectory starts to incline slightly away from the center of the container, which is not observed in the other flow patterns. At h = 45 mm, small bubbles begin to detach from the main bubble in the coupled buoyancy and thermocapillary flow scenario. This detachment becomes more pronounced with increasing h, eventually hindering the bubble's motion. By h = 90 mm, this interference leads to a significant reduction in flow, culminating in a complete cessation of motion at h = 120 mm. This behavior can be attributed to the opposing nature of gravitational and thermocapillary forces in these specific scenarios, where the buoyancy force starts to appear gradually from about h = 45 mm. In contrast, at smaller dimensions, these forces tend to work synergistically, enhancing bubble migration. Therefore, the selection of container dimensions plays a critical role in bubble migration dynamics when gravity is a factor, particularly at high Ma_T values.

Normal Gravity ($g=9.81 m/s^2$) | Normal Gravity & Thermocapillary | Thermocapillary (Marangoni effect)

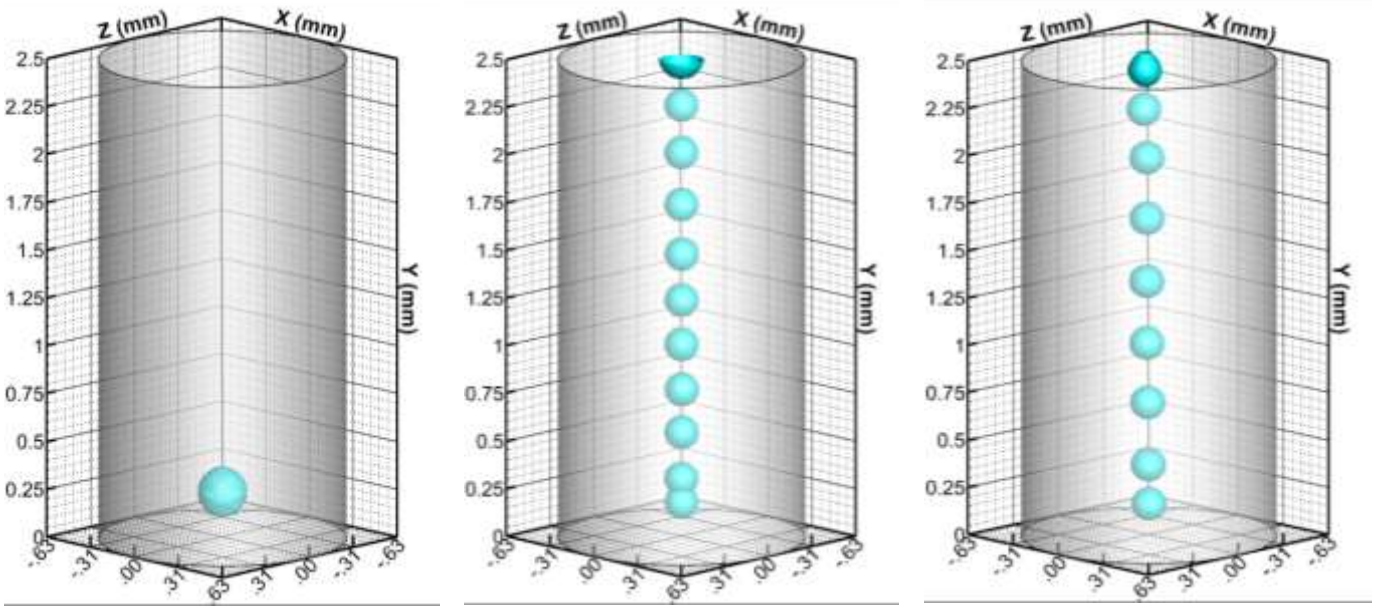

cylinder size 1.25 × 2.5 mm, r_b = 0.12 mm, No movement

cylinder size 1.25 × 2.5 mm, r_b = 0.08 mm, Ma_T = 51.5

cylinder size 1.25 × 2.5 mm, r_b = 0.08 mm, Ma_T = 51.5

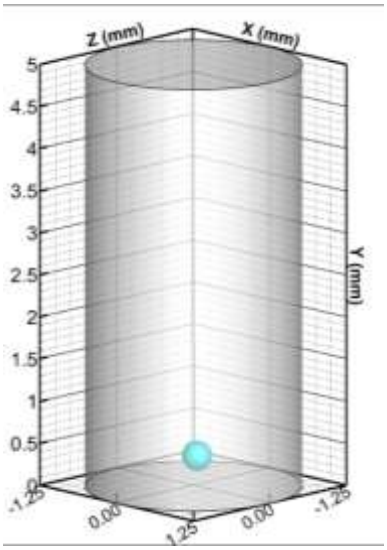

cylinder size 2.5 × 5 mm,
r_b = 0.16 mm (No movement)

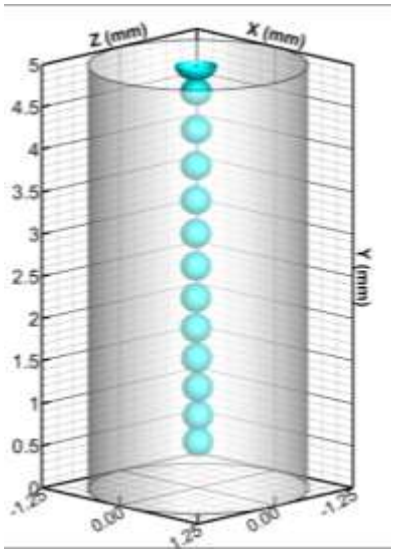

cylinder size 2.5 × 5 mm,
r_b = 0.16 mm, Ma_T = 102.9

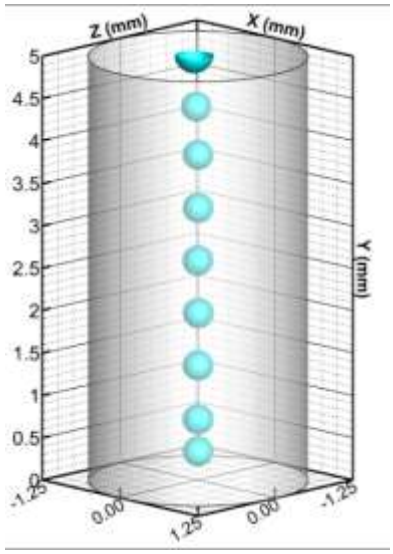

cylinder size 2.5 × 5 mm,
r_b = 0.16 mm, Ma_T = 102.9

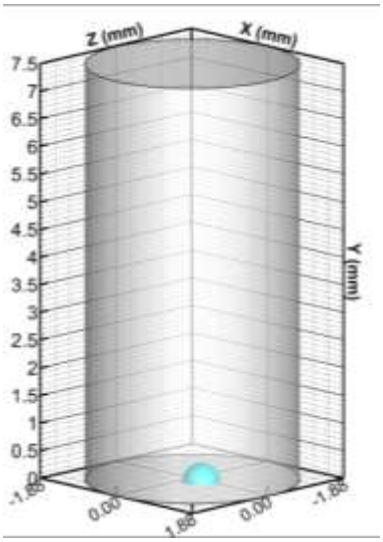

cylinder size 3.75 × 7.5 mm,
r_b = 0.24 mm No movement

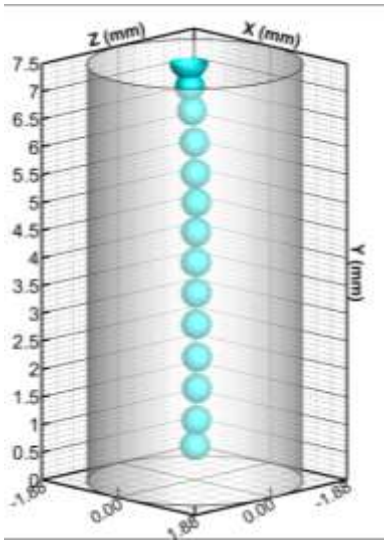

cylinder size 3.75 × 7.5 mm,
r_b = 0.24 mm, Ma_T = 154.4

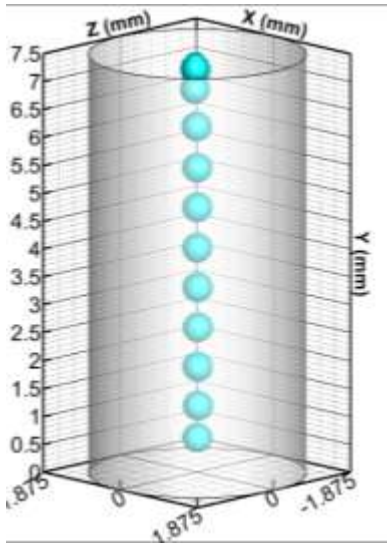

cylinder size 3.75 × 7.5 mm,
r_b = 0.24 mm, Ma_T = 154.4

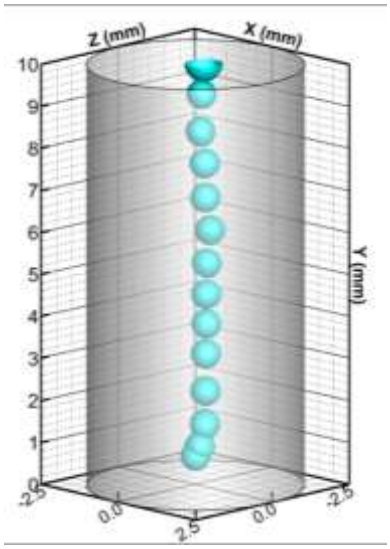

cylinder size 5 × 10 mm,
r_b = 0.32mm

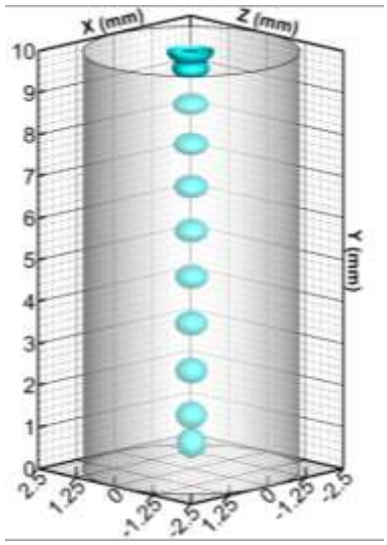

cylinder size 5 × 10 mm,
r_b=0.32mm, Ma_T=205.9

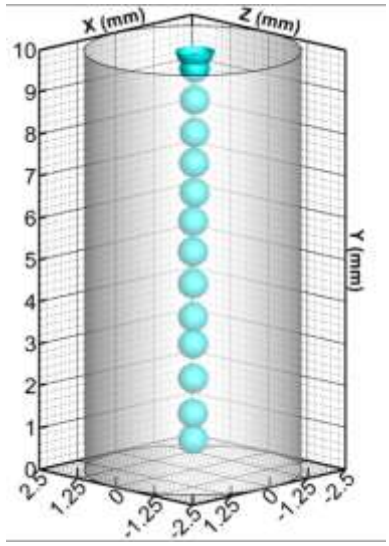

cylinder size 5×10 mm,
r_b=0.32mm, Ma_T=205.9

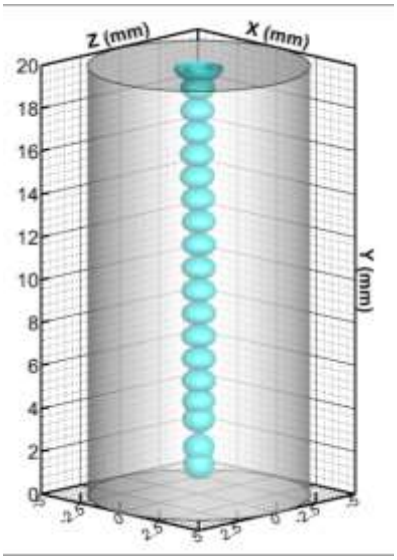

cylinder size 10 × 20 mm,
r_b = 0.64 mm

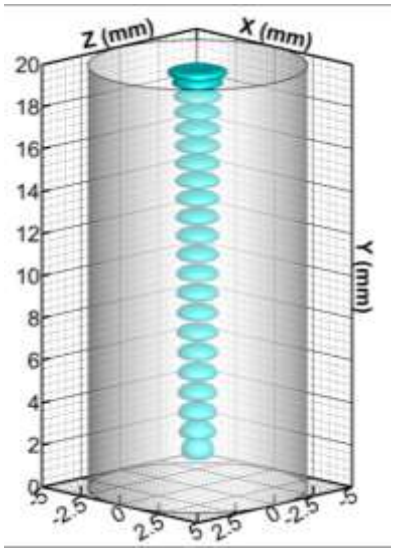

cylinder size 10 × 20 mm,
r_b = 0.64 mm, Ma_T = 411.7

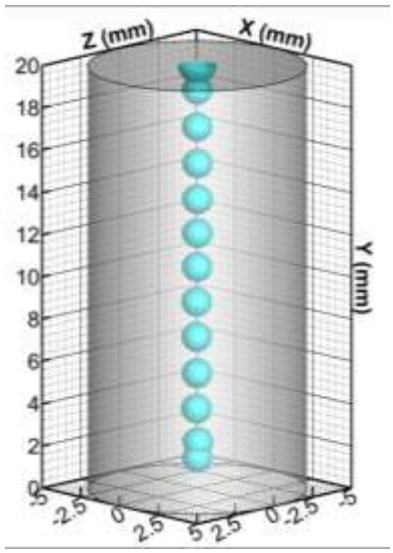

cylinder size 10 × 20 mm,
r_b = 0.64 mm, Ma_T = 411.7

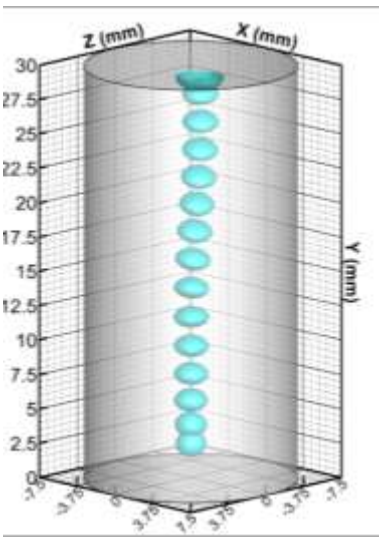

cylinder size 15 × 30 mm,
r_b = 0.96 mm

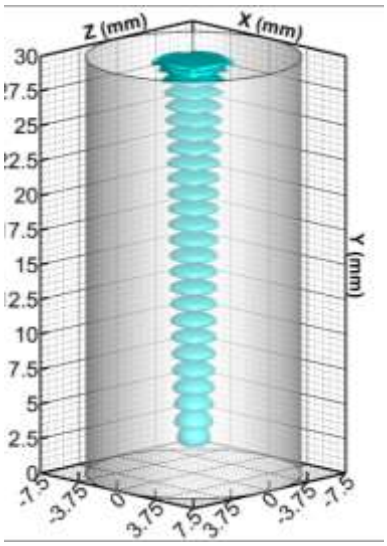

cylinder size 15 × 30 mm,
r_b = 0.96 mm, Ma_T = 617.6

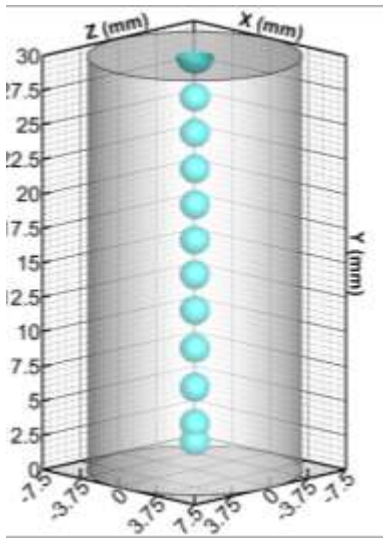

cylinder size 15 × 30 mm,
r_b = 0.96 mm, Ma_T = 617.6

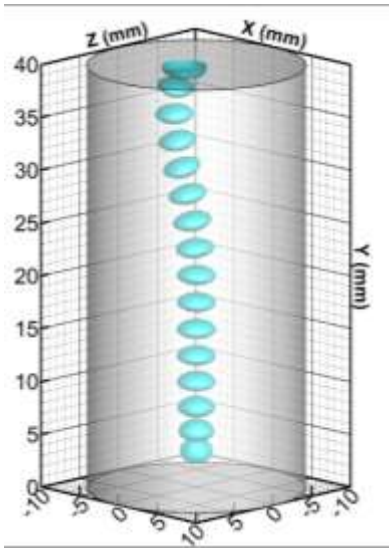

cylinder size 20 × 40 mm,
r_b = 1.28 mm

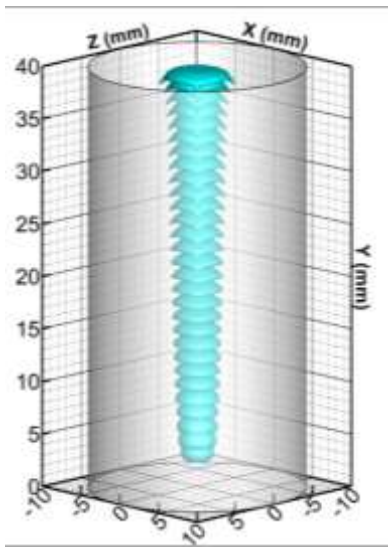

cylinder size 20 × 40 mm,
r_b = 1.28 mm, Ma_T = 823.4

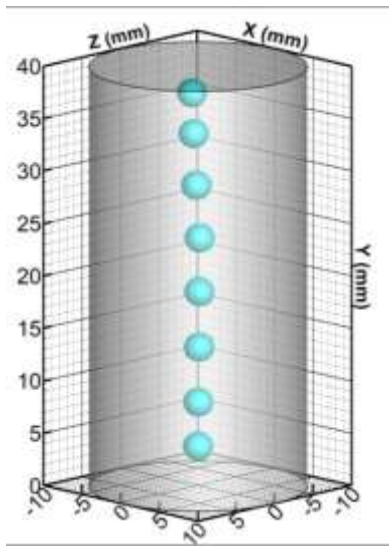

cylinder size 20 × 40 mm,
r_b = 1.28 mm, Ma_T = 823.4

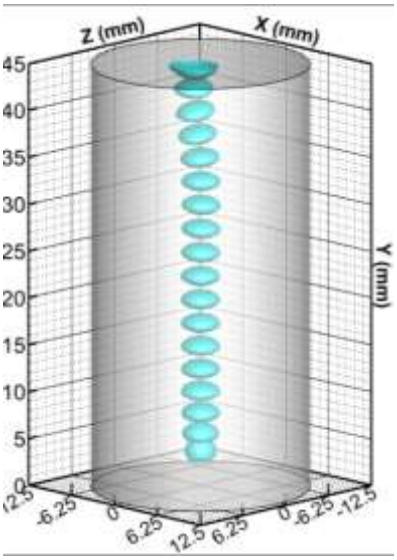

cylinder size 22.5 × 45 mm,
r_b = 1.44 mm

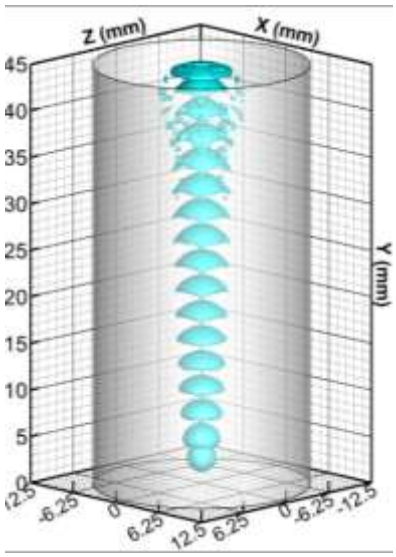

cylinder size 22.5 × 45 mm,
r_b = 1.44 mm, Ma_T = 926.3

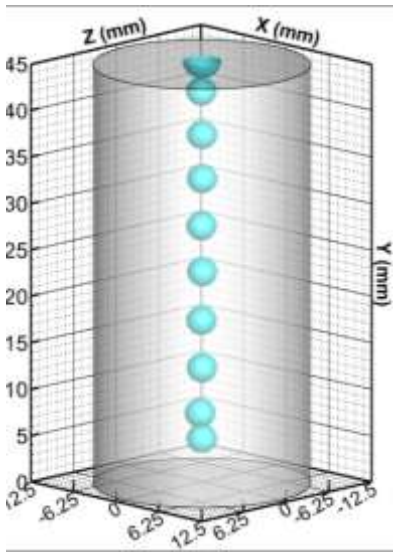

cylinder size 22.5 × 45 mm,
r_b = 1.44 mm, Ma_T = 926.3

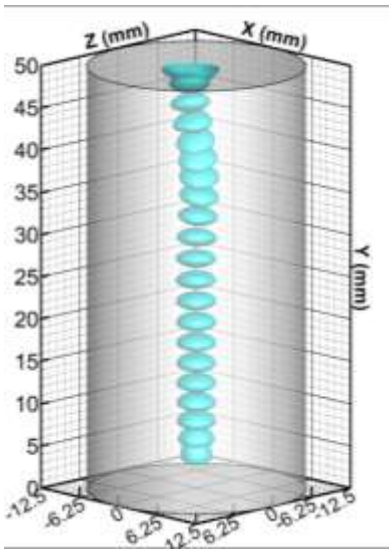

cylinder size 25 × 50 mm,
r_b = 1.6 mm

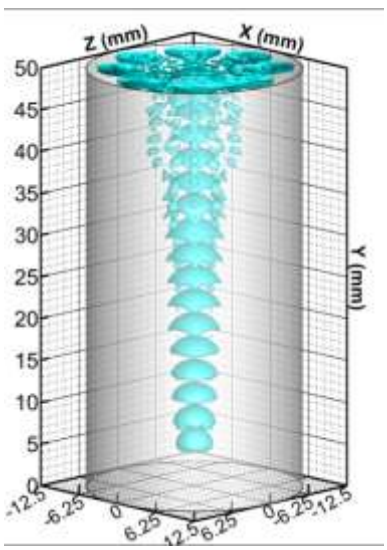

cylinder size 25 × 50 mm,
r_b = 1.6 mm, Ma_T = 1029.3

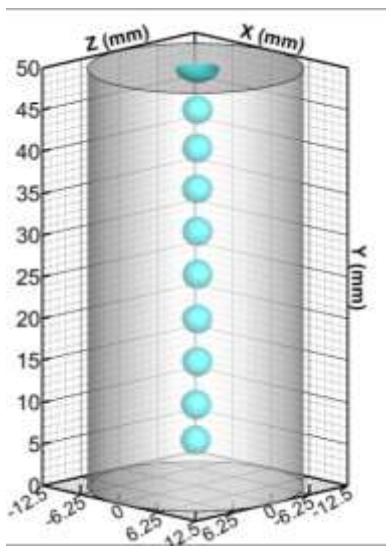

cylinder size 25 × 50 mm,
r_b = 1.6 mm, Ma_T = 1029.3

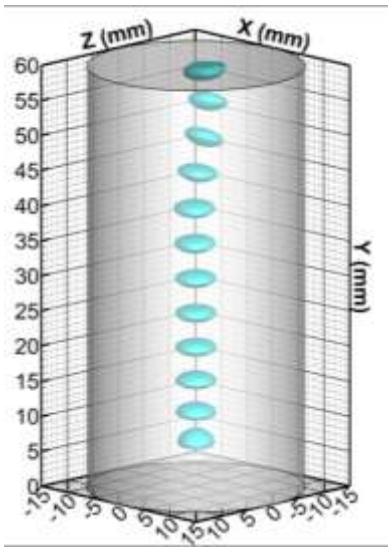

cylinder size 30 × 60 mm,
r_b = 1.92 mm

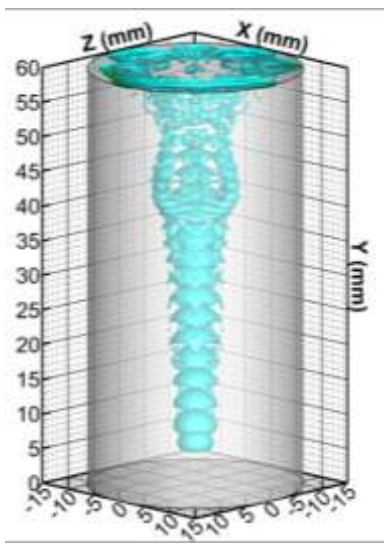

cylinder size 30 × 60 mm,
r_b = 1.92 mm, Ma_T = 1235

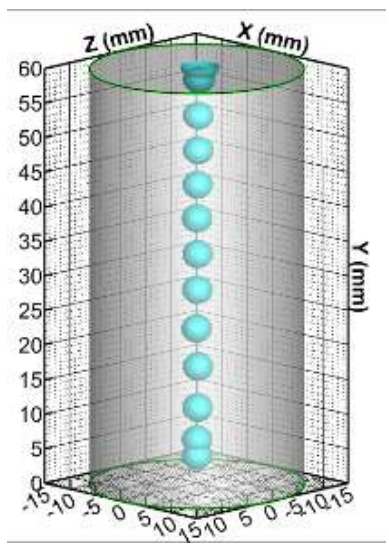

cylinder size 30 × 60 mm,
r_b = 1.92 mm, Ma_T = 1235

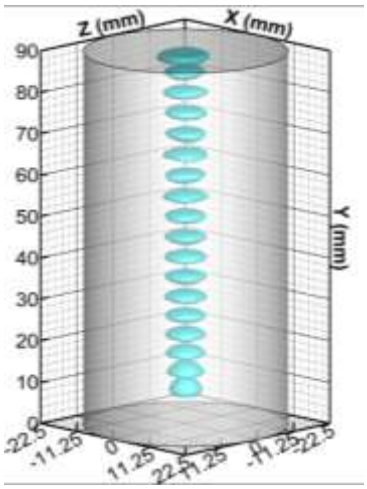

cylinder size 45 × 90 mm,
r_b = 2.88 mm

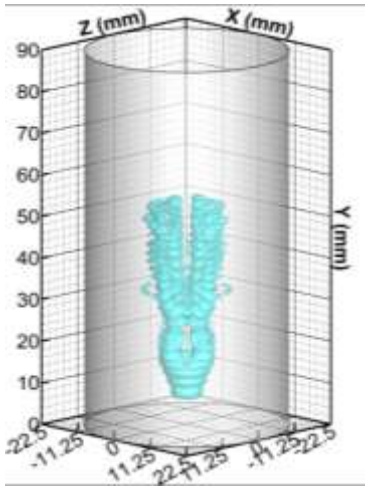

cylinder size 45 × 90 mm,
r_b = 2.88 mm, Ma_T = 1852.7

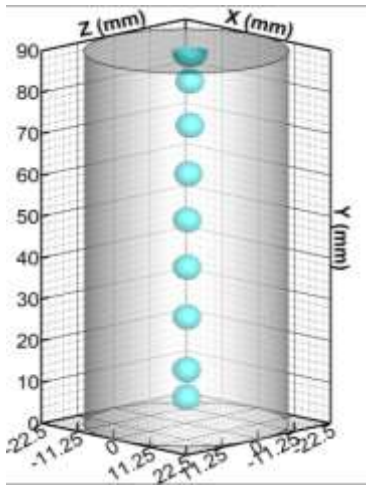

cylinder size 45 × 90 mm,
r_b = 2.88 mm, Ma_T = 1852.7

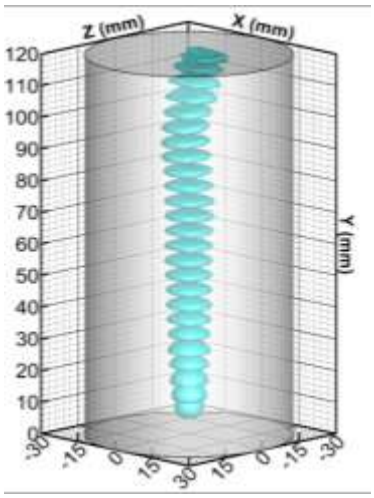

cylinder size 60 × 120 mm,
r_b = 3.84 mm

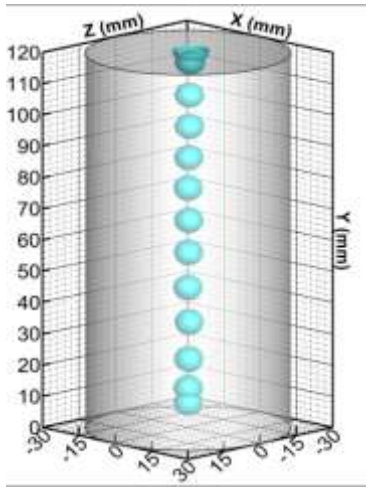

cylinder size 60 × 120 mm,
r_b = 3.84 mm, Ma_T = 2470

Figure 4. Bubble dynamics under thermocapillary force for different cylinder geometric dimensions with and without gravity

For fixed bubble radius (r_b = 0.48 mm) and surface temperatures maintained at 300 K (cold) and 325 K (hot), Figure 5 presents a comparison of bubble arrival times at the cylinder top under gravity, with and without thermocapillary effects. At h = 10 mm, the Marangoni effect dominates, enabling efficient bubble migration at such small scales. At h = 15 mm, buoyant forces begin to influence the motion, particularly in the cylinder's lower section. By h = 20 mm, buoyant forces clearly dominate, facilitating faster bubble migration. The relative contribution of thermocapillary forces diminishes as the container height increases.

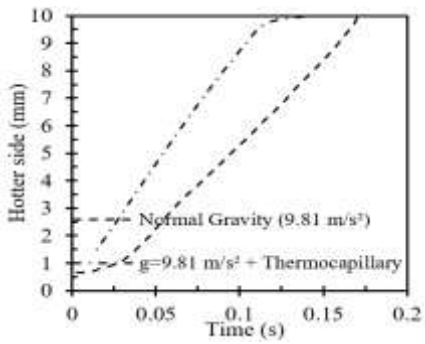

(a) h = 10 mm

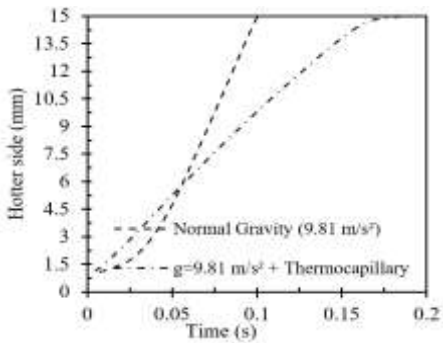

(b) h = 15 mm

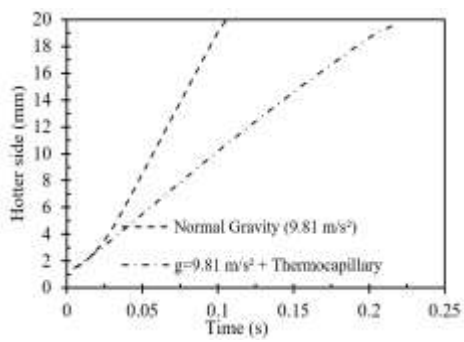

(c) h = 20 mm

Figure 5. Bubble migration arrival time to the top in normal gravity with and without thermocapillary force for Bubble radius = 0.48 mm

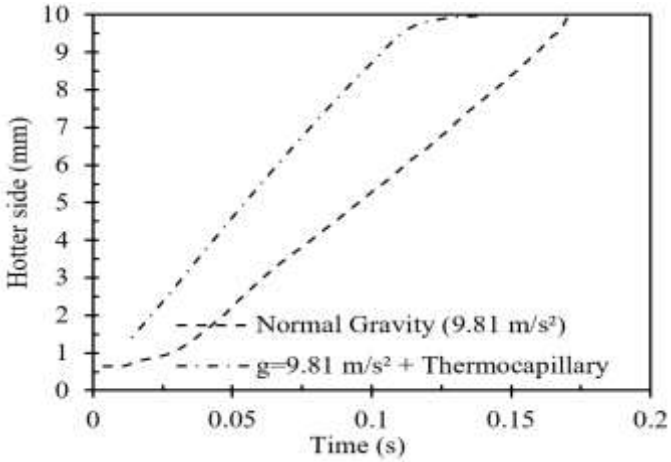

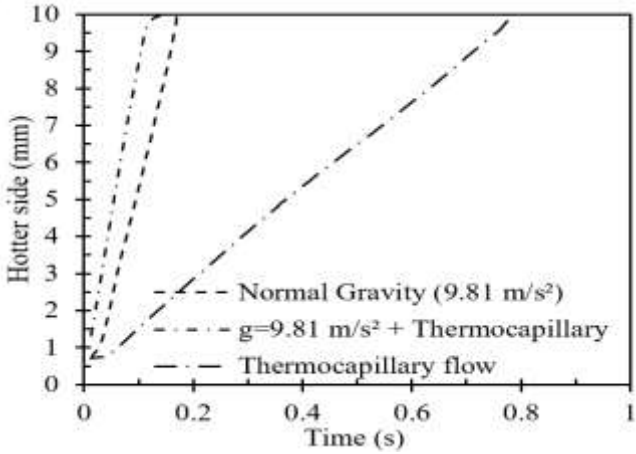

Cylinder height = 10 mm, Bubble radius = 0.32 mm

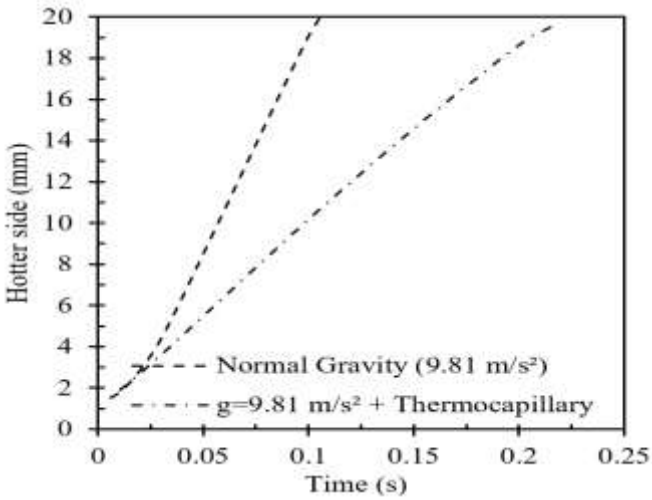

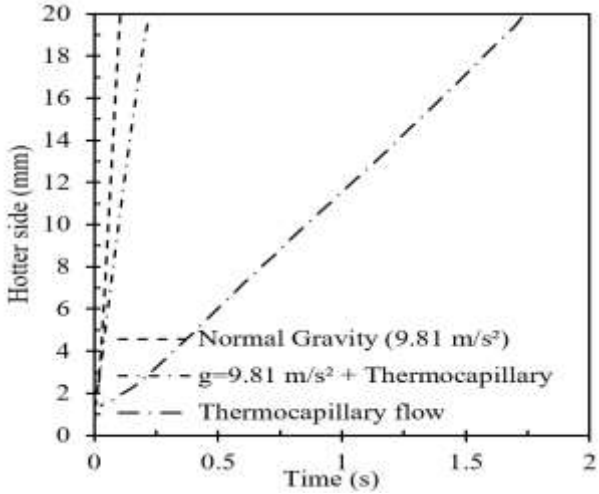

Cylinder height = 20 mm, Bubble radius = 0.64 mm

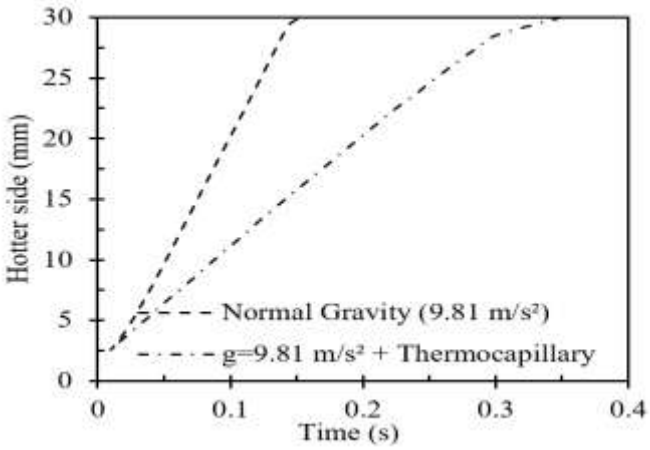

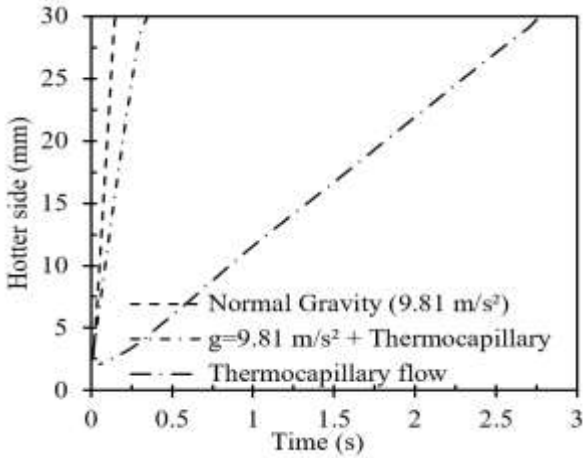

Cylinder height = 30 mm, Bubble radius = 0.96 mm

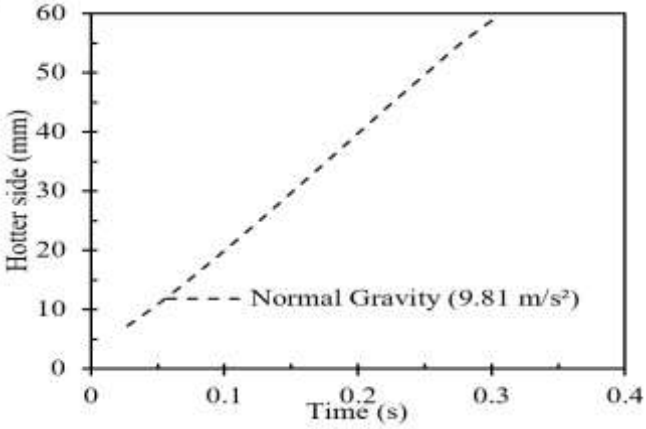

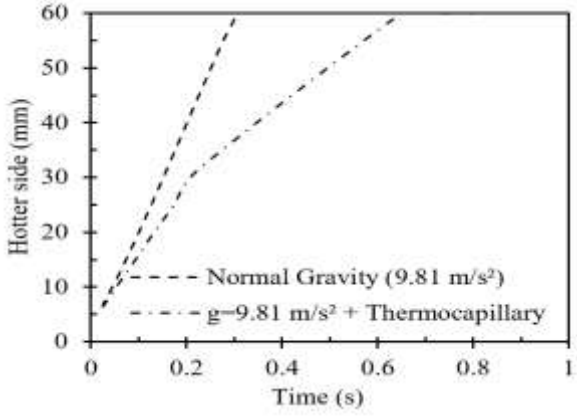

Cylinder height = 60 mm, Bubble radius = 1.92 mm

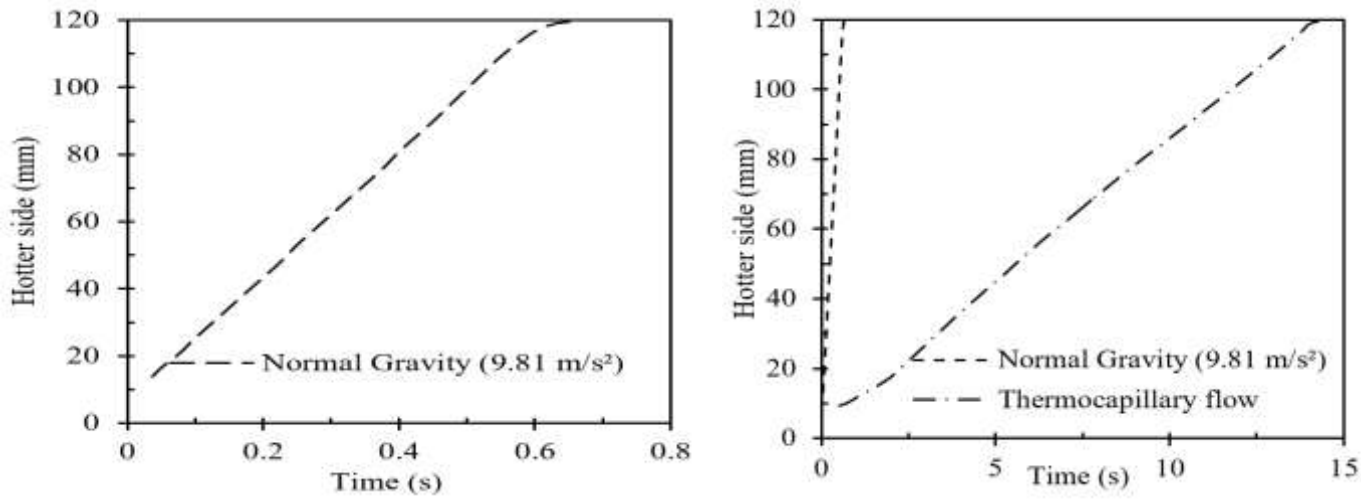

Figure 6. Bubble arrival time for different cylinder geometric dimensions under thermocapillary force with and without gravity presence

In Figure 6, variations in bubble diameter and container dimensions further clarify the interaction between thermocapillary and gravitational forces. In some instances, these forces do not combine effectively, resulting in the absence of their joint influence under specific conditions. For cylinder heights of h = 10 mm and h = 20 mm, the bubble's diameter has minimal impact on the dominant force driving its motion; instead, the height of the cylinder is the critical factor. The Marangoni effect is particularly pronounced in the presence of gravity, significantly reducing bubble arrival time at the cylinder's top for h = 10 mm. Beyond h = 20 mm, buoyant forces take precedence, accelerating bubble migration independently of thermocapillary effects.

Across all studied cylinder heights, thermocapillary forces alone consistently result in slower bubble migration compared to cases where buoyant forces are involved. In smaller cylinders, the interplay between buoyant and thermocapillary forces optimizes bubble travel time, emphasizing their synergistic contribution. However, in larger cylinders, buoyant forces alone emerge as the dominant mechanism, ensuring faster bubble motion.

These findings demonstrate the crucial role of container dimensions and force interactions in bubble migration dynamics. For small-scale systems, understanding and leveraging the interplay between thermocapillary and buoyant forces can enhance bubble control and efficiency. In larger systems, where buoyancy dominates, simplified models focusing on gravitational effects may suffice for predicting bubble behavior.

The results of this study have direct implications for several engineering and scientific applications. In microgravity environments, such as spacecraft thermal-control systems and propellant management units, buoyancy is negligible; therefore, thermocapillary forces can serve as an effective driving mechanism for bubble transport and removal. The present simulations show that for containers up to 10 mm in height and $r_b \leq 0.24$ mm, bubbles remain stationary under gravity alone but migrate fully under thermocapillary forces. This finding suggests that even modest temperature gradients ($\Delta T = 25$ K) can ensure continuous bubble removal and stable operation in compact heat-transfer devices in space.

In terrestrial small-scale systems, including microreactors and compact condensers, the dominance of thermocapillary forces below 10 mm and the transition to buoyancy at 20 mm provide a practical design guideline. To promote stable bubble transport, vertical distances should be kept below 10 mm or subdivided into short heated segments where thermocapillary motion assists buoyant rise. Conversely, in taller devices where buoyancy dominates, simpler gravity-based flow management can be applied.

For chemical and biomedical applications, these results highlight how the interplay between thermocapillary and gravitational forces affects both the arrival time and the shape of migrating bubbles. In chemical reactors or separation columns, combined thermocapillary and buoyant effects can enhance phase separation efficiency, while in biomedical microchannels, thermocapillary control could guide microbubbles for targeted drug delivery or localized heating without the excessive deformation observed under gravity-dominated conditions.

The model assumes an incompressible Newtonian liquid with constant properties and a linear dependence of surface tension on temperature. This approximation is appropriate for the small-scale cylinders studied here (height < 120 mm) and the modest temperature difference ($\Delta T = 25$ K), where property variations are minimal. A nonlinear σ_T relation or temperature-dependent viscosity could slightly alter the predicted bubble velocity but would not change the identified dominance of thermocapillary forces at $h \leq 10$ mm or buoyancy at $h \geq 20$ mm. Future work may include these refinements and limited experimental verification to confirm the robustness of the present findings.

The present study targets small cylindrical containers (height < 10 mm - 120 mm) with a hot top (325 K), cold bottom (300 K), and adiabatic sidewalls. The liquid was treated as incompressible and Newtonian, with constant thermophysical properties, while surface tension varied linearly with temperature. This simplification is widely used for narrow temperature ranges ($\Delta T = 25$ K) and small domains, and it isolates the thermocapillary mechanism effectively. We note, however, that if σ_T becomes nonlinear or temperature-dependent viscosity is considered, the quantitative magnitude of bubble velocity could change slightly, though the observed dominance trends (10 mm to 20 mm transition and deformation sequence) are expected to remain valid. Future numerical studies may examine nonlinear σ_T or temperature-

dependent viscosity to confirm sensitivity, and experimental validation under microgravity or confined conditions would help verify these trends.

7. CONCLUSION

A 3D model was created in Ansys-Fluent to investigate the effect of thermocapillary forces on the migration of a nitrogen bubble in small-scale containers under both normal and zero-gravity environments. The numerical model was validated by demonstrating strong agreement between the results obtained and those found in the literature. The findings demonstrate that:

- Thermocapillary forces can occur and have a significant impact when Earth's gravity is present, rather than being restricted to space and environments with no gravity.
- In the absence of gravity, the temperature gradient is the primary factor influencing the speed of bubble migration.
- Thermocapillary forces combined with gravity generally improve bubble movement in small-scale containers ≤ 10 mm in height, whereas for scales≥ 20 mm, gravity becomes the primary factor determining how quickly bubbles migrate.
- Under thermocapillary-only conditions, the bubble retains a near-spherical shape with slight elongation as it approaches the hot wall. Under gravity alone, the bubble becomes oblate, and the degree of flattening increases with r_b and h. With combined gravity and thermocapillary, flattening intensifies as size increases; small bubbles detach around $h = 45$ mm, motion weakens by $h = 90$ mm, and cease near $h = 120$mm. In buoyancy-driven flow, the trajectory tilts slightly off-center once $h > 20$ mm. These behaviors delineate the geometric ranges where thermocapillary forcing can be used to preserve shape and guide motion versus ranges where buoyancy dominates deformation and can impede migration.
- At a fixed bubble radius $r_b = 0.48$ mm, adding thermocapillary forces shortens the arrival time at $h = 10$ mm, compared with gravity alone; the benefit weakens at $h = 15$ mm. By $h = 20$ mm, gravity clearly yields the shortest arrival time, and adding thermocapillary effects does not further reduce it. Across all heights studied, thermocapillary-only motion is slower than cases where buoyancy is present. Moreover, for $h = 10$ and 20 mm, the container height, not bubble diameter, controls which mechanism sets the arrival time (diameter changes have minimal impact on the dominant mechanism). In cylinder height's < 10 mm, bubbles that are immobile under buoyancy alone at small sizes, $r_b \leq 0.24$ mm, do migrate when thermocapillary forces act.

The scale-dependent thresholds identified here also provide practical guidance for system design. In microgravity or confined geometries ($h \leq 10$ mm), thermocapillary forces can be used to accelerate bubble removal and stabilize two-phase heat-transfer processes. For larger configurations ($h \geq 20$ mm), buoyancy becomes the controlling mechanism, and device layouts should prioritize vertical alignment and venting paths for buoyant migration. These findings translate directly into improved performance and reliability for microgravity heat-transfer systems, chemical processing units, and biomedical microdevices.

ACKNOWLEDGMENT

We would like to express our gratitude for the support from the Kuwait Foundation for the Advancement of Sciences (KFAS).

REFERENCES

[1] Nie, D.M., Qiu, L.M., Zhang, X.B. (2015). Bubble motion under gravity through Lattice Boltzmann Method. In 2015 International Conference on Artificial Intelligence and Industrial Engineering, pp. 531-533. https://doi.org/10.2991/aiie-15.2015.142

[2] Nagasawa, S., Nomura, W., Miyata, Y., Fukuzawa, Y. (2001). Development of numerical simulator for a bubble behavior driven by Marangoni convection in viscous fluid under micro gravity. WIT Transactions on Modelling and Simulation, 29: 83-90. https://doi.org/10.2495/MB010081

[3] Jory, K., Satheesh, A. (2022). Marangoni convection in shallow annular pools of silicone oil heated from above. Case Studies in Thermal Engineering, 40: 102556. https://doi.org/10.1016/j.csite.2022.102556

[4] Kalichetty, S.S., Sundararajan, T., Pattamatta, A. (2019). Thermocapillary migration and interaction dynamics of droplets in a constricted domain. Physics of Fluids, 31(2): 022106. https://doi.org/10.1063/1.5084313

[5] Young, N.O., Goldstein, J.S., Block, M.J. (1959). The motion of bubbles in a vertical temperature gradient. Journal of Fluid Mechanics, 6(3): 350-356. https://doi.org/10.1017/S0022112059000684

[6] Hardy, S.C. (1979). The motion of bubbles in a vertical temperature gradient. Journal of Colloid and Interface Science, 69(1): 157-162. https://doi.org/10.1016/0021-9797(79)90090-0

[7] Bratukhin, Y.K., Kostarev, K.G., Viviani, A., Zuev, A.L. (2005). Experimental study of Marangoni bubble migration in normal gravity. Experiments in Fluids, 38(5): 594-605. https://doi.org/10.1007/s00348-005-0930-7

[8] Zheng, L., Zhang, X. (2017). Modeling and analysis of modern fluid problems. In Mathematics in Science and Engineering, Academic Press, pp. 39-77.

[9] Thompson, R.L., DeWitt, K.J., Labus, T.L. (1980). Marangoni bubble motion phenomenon in zero gravity. Chemical Engineering Communications, 5(5-6): 299-314. https://doi.org/10.1080/00986448008935971

[10] Annamalai, P., Shankar, N., Cole, R., Subramanian, R.S. (1982). Bubble migration inside a liquid drop in a space laboratory. Applied Scientific Research, 38(1): 179-186. https://doi.org/10.1007/BF00385947

[11] Balasubramaniam, R., Lacy, C.E., Woniak, G., Subramanian, R.S. (1996). Thermocapillary migration of bubbles and drops at moderate values of the Marangoni number in reduced gravity. Physics of Fluids, 8(4): 872-880. https://doi.org/10.1063/1.868868

[12] Hadland, P.H., Balasubramaniam, R., Wozniak, G., Subramanian, R.S. (1999). Thermocapillary migration of bubbles and drops at moderate to large Marangoni number and moderate Reynolds number in reduced gravity. Experiments in Fluids, 26(3): 240-248. https://doi.org/10.1007/s003480050285

[13] Xie, J.C., Lin, H., Zhang, P., Liu, F., Hu, W.R. (2005).

Experimental investigation on thermocapillary drop migration at large Marangoni number in reduced gravity. Journal of Colloid and Interface Science, 285(2): 737-743. https://doi.org/10.1016/j.jcis.2004.12.023
[14] Wozniak, G., Balasubramaniam, R., Hadland, P.H., Subramanian, R.S. (2001). Temperature fields in a liquid due to the thermocapillary motion of bubbles and drops. Experiments in Fluids, 31(1): 84-89. https://doi.org/10.1007/s003480000262
[15] Brackbill, J.U., Kothe, D.B., Zemach, C. (1992). A continuum method for modeling surface tension. Journal of Computational Physics, 100(2): 335-354. https://doi.org/10.1016/0021-9991(92)90240-Y
[16] Herrmann, M., Lopez, J.M., Brady, P., Raessi, M. (2008). Thermocapillary motion of deformable drops and bubbles. In Proceedings of the Summer Program. Center for Turbulence Research, USA, pp. 155-170.
[17] Alhendal, Y., Turan, A., Hollingsworth, P. (2013). Thermocapillary simulation of single bubble dynamics in zero gravity. Acta Astronautica, 88: 108-115. https://doi.org/10.1016/j.actaastro.2013.03.017
[18] Kumar, R., Lin, Y.C., Lin, C.W., Lin, M.C., Hsu, H.Y. (2022). An analysis of bubble migration in horizontal thermo-capillarity using the VOF modeling. Applied Sciences, 12(9): 4355. https://doi.org/10.3390/app12094355
[19] Hirt, C.W., Nichols, B.D. (1981). Volume of fluid (VOF) method for the dynamics of free boundaries. Journal of Computational Physics, 39(1): 201-225. https://doi.org/10.1016/0021-9991(81)90145-5
[20] Tomiyama, A., Zun, I., Sou, A., Sakaguchi, T. (1993). Numerical analysis of bubble motion with the VOF method. Nuclear Engineering and Design, 141(1-2): 69-82. https://doi.org/10.1016/0029-5493(93)90093-O
[21] Alhendal, Y., Turan, A. (2015). Thermocapillary bubble dynamics in a 2D axis swirl domain. Heat and Mass Transfer, 51(4): 529-542. https://doi.org/10.1007/s00231-014-1427-9
[22] Alhendal, Y., Turan, A., Kalendar, A. (2017). Wall effects on the thermocapillary migration of single gas bubbles in stagnant liquids. Heat and Mass Transfer, 53(4): 1315-1326. https://doi.org/10.1007/s00231-016-1903-5
[23] Balcázar, N., Oliva, A., Rigola, J. (2016). A level-set method for thermal motion of bubbles and droplets. In Journal of Physics: Conference Series, 745(3): 032113. https://doi.org/10.1088/1742-6596/745/3/032113
[24] Alhendal, Y., Turan, A., Kalendar, A. (2016). Thermocapillary migration of an isolated droplet and interaction of two droplets in zero gravity. Acta Astronautica, 126: 265-274. https://doi.org/10.1016/j.actaastro.2016.05.001
[25] Mahmoudi, S., Saeedipour, M., Hlawitschka, M.W. (2024). Bubble dynamics under the influence of the Marangoni force induced by a stratified field of contamination. Experimental and Computational Multiphase Flow, 6(4): 353-364. https://doi.org/10.1007/s42757-023-0182-x
[26] Yamaguchi, T., Iguchi, M., Uemura, T. (2004). Behavior of a small single bubble rising in a rotating flow field. Experimental Mechanics, 44(5): 533-540. https://doi.org/10.1007/BF02427965
[27] Alhendal, Y., Turan, A., Al-Mazidi, M. (2015). Thermocapillary bubble flow and coalescence in a rotating cylinder: A 3D study. Acta Astronautica, 117: 484-496. https://doi.org/10.1016/j.actaastro.2015.09.009
[28] Alhendal, Y. (2024). Influence of temperature gradients and fluid vibrations on the thermocapillary droplet behavior in a rotating cylinder. Heat Transfer Research, 55(9): 71-90. https://doi.org/10.1615/heattransres.2024051366
[29] Alhendal, Y., Touzani, S. (2025). Thermocapillary bubble movement in a vibrating fluid inside a rotating cylinder. Multiphase Science and Technology, 37(1): 41-56. https://doi.org/10.1615/multscientechn.2024055659
[30] Movassat, M., Ashgriz, N., Bussmann, M. (2009). Bubble dynamics under forced oscillation in microgravity environment. In ASME International Mechanical Engineering Congress and Exposition. Heat Transfer, Fluid Flows, and Thermal Systems, Parts A, B and C. Lake Buena Vista, Florida, USA, 9: 1787-1793. https://doi.org/10.1115/IMECE2009-12616
[31] Alhendal, Y., Touzani, S., Turan, A., Cheddadi, A. (2023). Thermocapillary bubble oscillations and migration in a vibrating cylinder in a zero-gravity environment. Microgravity Science and Technology, 35(3): 22. https://doi.org/10.1007/s12217-023-10046-z
[32] Alhendal, Y., Touzani, S. (2024). Impact of heat flow from the cylinder sidewalls on thermocapillary droplet flow in a vibrating fluid: 3D study. Heat and Mass Transfer, 60(8): 1429-1440. https://doi.org/10.1007/s00231-024-03499-4
[33] Ma, X. (1999). Numerical simulation of thermocapillary drop motion with internal circulation. Numerical Heat Transfer: Part A: Applications, 35(3): 291-309. https://doi.org/10.1080/104077899275254
[34] Sussman, M., Puckett, E.G. (2000). A coupled level set and volume-of-fluid method for computing 3D and axisymmetric incompressible two-phase flows. Journal of Computational Physics, 162(2): 301-337. https://doi.org/10.1006/jcph.2000.6537
[35] Ma, Y., Cheng, Y., Shen, Y., Xu, J., Sui, Y. (2020). Manipulation of bubble migration through thermal capillary effect under variable buoyancy. International Journal of Thermal Sciences, 149: 106199. https://doi.org/10.1016/j.ijthermalsci.2019.106199
[36] Balla, M., Tripathi, M.K., Sahu, K.C., Karapetsas, G., Matar, O.K. (2019). Non-isothermal bubble rise dynamics in a self-rewetting fluid: Three-dimensional effects. Journal of Fluid Mechanics, 858: 689-713. https://doi.org/10.1017/jfm.2018.774
[37] Clift, R., Grace, J.R., Weber, M.E. (1978). Bubbles, Drops and Particles. Academic Press, New York.
[38] Youngs, D.L. (1982). Time-dependent multi-material flow with large fluid distortion. Numerical Methods for Fluid Dynamics, Academic Press, pp. 273-285.
[39] Cohen, C., Darbois Texier, B., Reyssat, E., Snoeijer, J. H., Quéré, D., Clanet, C. (2017). On the shape of giant soap bubbles. Proceedings of the National Academy of Sciences, 114(10): 2515-2519. https://doi.org/10.1073/pnas.1616904114

NOMENCLATURE

CFD	computational fluid dynamics
VOF	volume of fluid
PLIC	piece-wise linear interface calculation

YGB	young, Goldstein, and block model
CSF	continuum surface force
div	divergence ($\nabla \cdot \mathbf{u} = \frac{\partial u}{\partial x} + \frac{\partial v}{\partial y} + \frac{\partial w}{\partial z}$)
PISO	Pressure-Implicit with Splitting of Operators
PRESTO	Pressure-Staggering Option
d	diameter, m
3D	three dimensions
r	radius, m
V_T	thermal velocity, ms^{-1}
E	energy, joule
g	gravitational acceleration, $m.s^{-2}$
h	Heat transfer coefficient, $w.m^{-2}.\ k^{-1}$
k	thermal conductivity, $w.m^{-1}.\ k^{-1}$
k	local surface curvature
Pr	Prandtl number, dimensionless
Pe	Peclet number, dimensionless
$\vec{n}$	surface normal
d	differential
Re_T	thermal Reynolds number, dimensionless
Ma_T	thermal Marangoni number, dimensionless
s	source term
T	temperature, K
T_o	reference temperature, K
t	time, s
$\vec{v}$	velocity vector, (u_1, u_2, u_3)
x	x coordinate, m
y	y coordinate, m
mm	millimeter, mm

Greek symbols

ρ	density, kg/m^3
α	thermal diffusivity, $m^2.s^{-1}$
μ	dynamic viscosity, $kg.m^{-1}.s^{-1}$
λ	thermal conductivity, $W.m^{-1}.K^{-1}$
∂	rate of change
σ	surface tension, $N.\ m^{-1}$
σ_o	surface tension at a reference temperature

Subscripts

b	bubble, m
T	Temperature, K
x	local distance, m
G	gas
o	reference
eff	effective thermal conductivity